Journal of Molecular Structure 1291 (2023) 136098

Contents lists available at ScienceDirect

Journal of Molecular Structure

journal homepage: www.elsevier.com/locate/molstr

Exploring microstructure of $MgCl_2$·nEtOH adducts for Ziegler-Natta catalysts

Reza Bazvand [a], Naeimeh Bahri-Laleh [a], Hossein Abedini [a,*], Mehdi Nekoomanesh [a], Albert Poater [b,*]

[a] Iran Polymer and Petrochemical Institute (IPPI), P.O. Box 14965/115, Tehran, Iran
[b] Institut de Química Computacional i Catàlisi, Departament de Química, Universitat de Girona, c/ Mª Aurèlia Capmany 69, Girona, Catalonia 17003, Spain

ARTICLE INFO

Keywords:
Ziegler-natta catalyst
EtOH/$MgCl_2$ adduct
Polyolefins
Alcohol amount

ABSTRACT

The activation of $MgCl_2$ through the formation of $MgCl_2$·nEtOH adducts is considered the principal step for the preparation of high performance Ziegler-Natta catalysts for olefins polymerizations in industry. Despite this importance, due to the complicated microstructure of the adducts, the precise structural characterization of these compounds has been left behind. In this research, four $MgCl_2$.nEtOH adducts (with n = 0.6, 1.0, 1.8, and 3.2) were prepared by melt quenching procedure and assessed thoroughly by different techniques. Despite the multiple peaks in TGA analysis, similar FTIR spectra were recorded, and the adducts with n = 3.2 revealed sticky nature in SEM pictures which enhanced their particle size and broadened SPAN. According to the XRD spectra, the adducts showed distinct peaks related to the lateral cuts of distorted $MgCl_2$, in which the ratio of α-$MgCl_2$ to β-$MgCl_2$ form enhanced by increasing the EtOH content, that was further confirmed by DFT calculations, even though it must be accepted that it is only a minimalist exercise in terms of a clear characterization of the adducts.

1. Introduction

Today, polyethylene (PE) and polypropylene (PP) are considered the largest volume synthetic polymers in the world. Their related business accounts for over than 60% of the total plastics market with an annual production of more than 160 million tons [1,2]. The demand for these plastics is steadily growing [3], thanks to the facile availability of raw materials, the low production expense, and the excellent polymer characteristics which enable their simple adaption for vast kinds of applications ranging from packaging, films, piping, to the pharmaceutical, oil and automotive industries [4–7].

The advent of Ziegler-Natta catalysts for the polymerization of ethylene and propylene in 1953 is undoubtedly one of the major events of the 20th century that influenced the polymer industry [8,9]. The so called catalysts have a fundamentally heterogeneous nature [10], employed for the industrial production of different types of PEs and PPs, thanks to their prodigious catalyst activity, easy and economically preparation process, suitable polymer morphology, good stereo-selectivity and high polyolefin molar mass control ability [11–13]. Despite great achievements in the industrial production of advanced polyolefin materials and advent of new high performance technologies [14], an intimate understanding of the catalysts nanostructure has remained elusive until now [15,16]. This shortcoming arises from the multisite nature of the final catalyst, which itself originates from the complex structure of the related support [17,18]. Indeed, the catalyst particles behavior during polymerization as well as final properties of furnished polymer originates mainly from the nanostructure of primary support, according to the well-known replication phenomenon [19,20]. In fact, the Ziegler-Natta catalysts' extraordinary success in polyolefin industry is due to the usage of $MgCl_2$ support comprising multigrain and porous spherical particles [21–23], apart from other (early) transition metal based catalysts [24–27], particularly with high interest on polyalphaolefins [6,28–31]. This special kind of structure of $MgCl_2$ imposes a controlled fragmentation during the polymerization experiment that results into the formation of polymer particles with favorable morphology [32–34].

It is generally accepted that $MgCl_2$ can exist in nature in three different crystalline forms including α, β and δ. According to the literature, commercial $MgCl_2$ contains either α structure in which the Cl anions are packed into a face-centered cubic (fcc) unit, or the β form in which the Cl anions are packed in a hexagonal close packing (hcp) unit [35–37]. As a consequence, the arrangement of the chlorine atoms in the

* Corresponding authors.
E-mail addresses: h.abedini@ippi.ac.ir (H. Abedini), albert.poater@udg.edu (A. Poater).

https://doi.org/10.1016/j.molstruc.2023.136098
Received 16 May 2023; Received in revised form 23 June 2023; Accepted 24 June 2023
Available online 25 June 2023

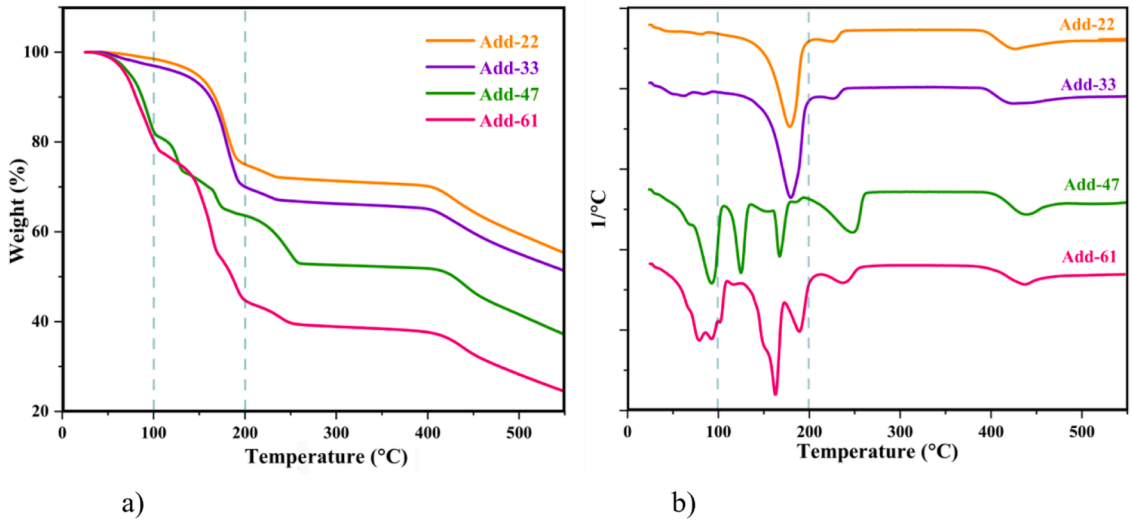

Fig. 1. (a) TGA and (b) DTGA curves obtained from thermal analysis.

stacking direction differs from ABCABC in the α form to the ABAB in the β form [38].

Primary $MgCl_2$ is not active for $TiCl_4$ adsorption, as the active site of the Ziegler-Natta catalyst, considering experimental [39–41] or theoretical insights [42]. Its activation via chemical or physical routes leads to the formation of small $MgCl_2$ crystallites with a large surface area and special crystalline surfaces. Among the possible lateral cuts termination of $MgCl_2$, the (001), (110), (015) and (104) facets are the most classically considered ones in the literature [20,43]. These surfaces encompass various electronic environments that imposes different behavior on the furnished $MgCl_2/TiCl_4$ active sites [44–46].

Among the suggested procedures for the $MgCl_2$ activation, the chemical route employing a Lewis base compound, generally ethanol (EtOH), is well accepted in both industry and academy [47,48]. Via this method, appropriate $MgCl_2$·EtOH adducts suitable for catalyst impregnation are prepared. In this regard, the ethanol extent plays a dominant role in tuning the pore texture in the final Ziegler-Natta catalysts. The identification of the molecular structure of $MgCl_2$ crystallites relevant for the synthesis of Ziegler-Natta catalysts has been the subject of several experimental and computational investigations [40,49–51] so far. However, the more challenging topic of this subject still remains the true microstructure of $MgCl_2$·EtOH adducts containing different amounts of alcohol, particularly their characterization [35,44,52–57]. In the current research we will try to fill this gap. It should be pointed out that the word "microstructure" is used here for the structure of the $MgCl_2$·nEtOH catalyst adducts, which would generally be a term formally referring to polymers obtained by heterogeneous Ziegler-Natta (ZN) systems [38, 58]. In this regard, the microstructure of four adducts with different ethanol contents is assessed by different analytical tools to unravel the effect of alcohol treatment on the overall characteristics. In addition, to stress that the preparation of suitable adducts may have significant effects also on the $TiCl_4$ active site dynamics on the ZN surfaces [59–61].

2. Experimental

2.1. Materials

All the chemicals were purchased from Aldrich Co, Germany. Hexane and toluene were distilled over Na/ benzophenone, prior to use. The other materials were used in as received form.

2.2. Adducts preparation experiments

Preparation of adduct samples was accomplished according to the method described in our recent publication [62]. In a brief procedure, three round bottom glass balloons were utilized consecutively. 10 g (105 mmol) $MgCl_2$ is melted in 19.6 mL EtOH (336 mmol, EtOH/$MgCl_2$=3.2) at the first balloon containing 10 g silicon oil, at T = 67 °C during 8 h. the temperature was raised to 110 °C, 25 g silicon oil was added to the mixture with continuous stirring to reach a homogenous dispersion. After 2 h, the content of first balloon was transferred into the second balloon containing 500 mL of cold hexane at T=-15 °C. After 1 h continuous stirring, the solvent above solid product was evacuated. The solid product was washed with cold hexane and then underwent thermal dealcoholation in a fluidized reactor utilizing N_2 flow, to furnish final $MgCl_2$.nEtOH adducts.

2.3. Characterization

Particle size and adduct distribution were measured applying a Malvern Zetasizer Nano ZS instrument (United Kingdom) according to ISO 13,320–2 standard. X-ray diffraction (XRD) analysis was performed using Siemens D-5000 X-ray diffractometer (USA) at 40 kV and 25 mA with a copper target (λ = 1.54 Å) and at a scanning rate of 3°/min. SEM images of the synthesized adducts and also EDX maps were acquired using SEM model S-3000 N, Hitachi (Japan) instrument. Thermogravimetric analysis (TGA) was conducted to obtain EtOH content of adducts, utilizing Mettler Toledo Inc. (Switzerland) instrument under N_2 atmosphere with a heating rate of 10 °C/min. The specific surface area of adducts was calculated employing Brunauer–Emmett–Teller (BET) analyzer using a BELSORP Mini II instrument.

Fourier transform infrared spectroscopy (FTIR) was performed employing the BRUKER, EQUINOX 55 tool instrument using KBr pellets prepared in the glove-box to avoid humidity impact.

It is worth noting that, to avoid water contamination during the characterizations, all sample preparations were performed in the glove box under a nitrogen atmosphere.

2.4. Computational details

Density Functional Theory (DFT) calculations were carried out with the Gaussian16 package [63]. The geometry optimizations were performed without symmetry constraints via the spin-restricted Kohn-Sham (RKS) formalism and employing the B3LYP-D3, hybrid GGA functional of Becke-Lee, Parr, and Yang [64–66], with the Grimme D3 correction term to the electronic energy [67]. The triple-zeta polarization basis set Def2-TZVP keyword was used for all atoms [68,69]. Frequency calculations were carried out to approve the nature of the stationary points

Table 1
Particle size data of the studied adducts.

	EtOH (%)	n[1]	d10 (μm)[2]	d50 (μm)[2]	d90 (μm)[2]	SPAN[3]
Add-22	22	0.6	18	35	70	1.5
Add-33	33	1.0	20	36	67	1.3
Add-47	47	1.8	20	38	70	1.3
Add-61	61	3.2	10	40	111	2.5

[1] molar ratio of ethanol to $MgCl_2$,.
[2] d10, d50 and d90 represent the size point below which 10, 50 and 90% of adducts are contained, respectively.
[3] SPAN=(d90-d10)/d50.

(minima without imaginary frequencies). Geometry optimizations were performed with and without solvent effects. When they were considered, the approach was based on the polarizable solvation model (SMD), variation of IEFPCM of Truhlar and co-workers [70], using ethanol as solvent.

3. Results and discussion

Four different $MgCl_2$·nEtOH adducts, with various $MgCl_2$/EtOH molar ratios, were prepared according to the method mentioned in a previous study by some of us [62]. To examine the amount of adsorbed alcohol, in Fig. 1a TGA analysis was employed under nitrogen atmosphere, while in Fig. 1b DTGA thermograms were obtained by differentiating TGA thermograms. By employing TGA curves, various ethanol extent with n = 0.6, 1.0, 1.8, and 3.2 were calculated for Add-22, Add-33, Add-47 and Add-61, respectively. According to the curves, two distinctive weight losses were indicated for the adducts with n<1 at the temperatures of 189 and 230 °C, corresponding to the desorption of EtOH from $MgCl_2$ support. On the other hand, in the Add-47 and Add-61 cases comprising a higher content of ethanol (n>1.8), some other peaks were observed at lower temperatures of < 140 °C indicating a loose binding of ethanol to the support. In fact, in the case of adducts with higher stoichiometry ratio of alcohol, lower ethanol dissociation temperature was detected. The temperature is close to the boiling point of free ethanol, which confirms a very weak association of ethanol with the matrix comprising a high ethanol content. It causes the free movement of ethanol between $MgCl_2$ surfaces even at room temperature [71].

Dynamic light scattering (LPS) analysis was employed to investigate adducts particle sizes and their related distributions, that is reported as the SPAN parameter in Table 1 and Fig. 2. Notably, no significant difference was found in the d10, d50, d90 and SPAN of the adduct samples containing less than 47 wt.% of ethanol. Indeed, these adducts had an identical d50 of 35–38 μm and a narrow SPAN of 1.3–1.5, which are normal for appropriate commercial gas phase polyolefin catalysts. However, in the Add-57 case, d10 decreased, while d90 increased at larger particle sizes, due to the sticky nature of the adducts with high ethanol content. It causes agglomeration of small size particles with the others during LPS analysis as well as their storage resulting in deformed structures. The advent of a small peak at the large particle sizes in the Add-61 sample (Fig. 2a) confirms this deduction which was further confirmed by widening the SPAN value to 2.5.

SEM analysis was employed to unravel the morphology of the studied adducts. It is clear from Fig. 3 that all adduct samples have a spherical shape, which is privileged for industrial sectors, due to easy handling and transport of catalyst and polymer particles in the gas phase polymerization reactors as well as related down-stream sectors. In particular, the agglomeration of adduct samples containing 61% ethanol is clear in the related SEM picture (Fig. 3c), due to their extremely sticky nature. This phenomenon may be the origin of the peak observed at larger particle diameters in LPS diagram of Add-61 sample (Fig. 3a). As a consequence, special caution should be taken for the storage and handling of adducts comprising a large amount of ethanol.

In the EDX mappings in Fig. 3, the presence of Mg, Cl, and C is confirmed in which Mg and Cl are indicative of the $MgCl_2$ support and C corresponds to the ethanol precursor. All maps disclosed the uniform dispersion of elements in adduct textures.

XRD analysis was performed on the studied adducts and the patterns were compared with those of primary $MgCl_2$. In the XRD pattern of neat $MgCl_2$, some distinctive peaks can be observed at 2θ angles of 16 ° (correlated to the Cl–Mg–Cl triple layers along the crystallographic direction which represents (003) plane), 31, 33, 34 and 50 ° (correspond to the (012), (011), (104) and (110), respectively) [72], Fig. 4. Among those facets, the (003) surface is correlated to the basal plane comprising only Cl atoms, so, it is not considered as suitable plane for $TiCl_4$ adoption [21]. Moving to the adduct samples, the stacking order affected the (003) diffraction peak. Indeed, the (003) peak almost disappeared, while some peaks were emerged at 2θ angles in the range of 20–30° It was demonstrated that the complete shift of the peak at 2θ =16° is indicative of Cl-Mg-Cl mono layers [7]. On the other hand, the intensity of the peak at 2θ =34°, correlated to the (004) plane, enhanced in favor of catalyst precursor impregnation. In fact, in the (104) and (110) planes the Mg^{+2} ions have a penta- and tetra-coordinated nature, respectively, corresponding to one and two vacancies relative to the 6-coordinated magnesium atoms in the (003) plane and in the bulk [23].

Our finding here is in agreement with the accepted idea that

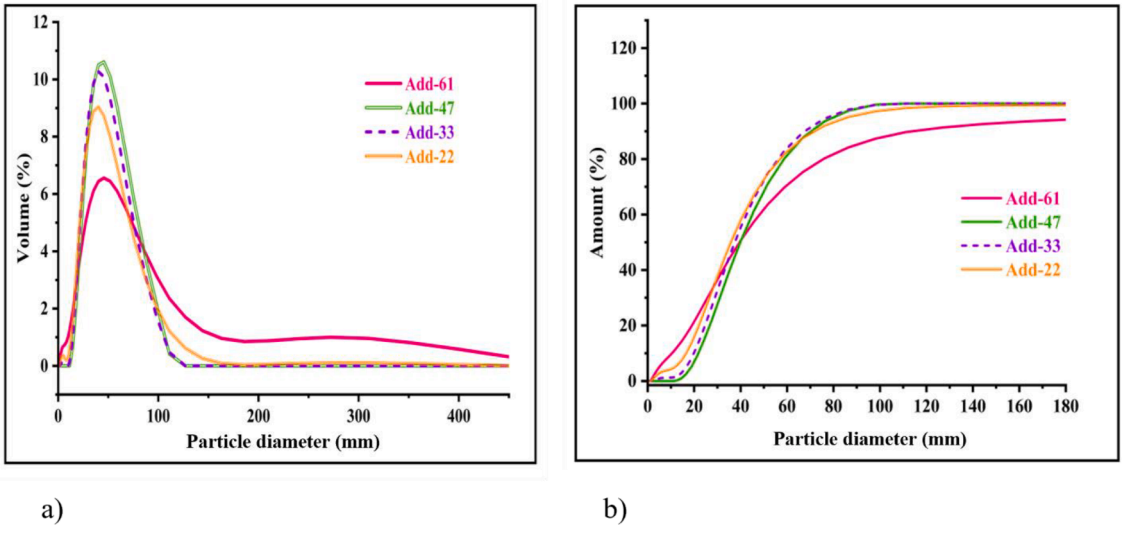

Fig. 2. Adducts particle size distribution.

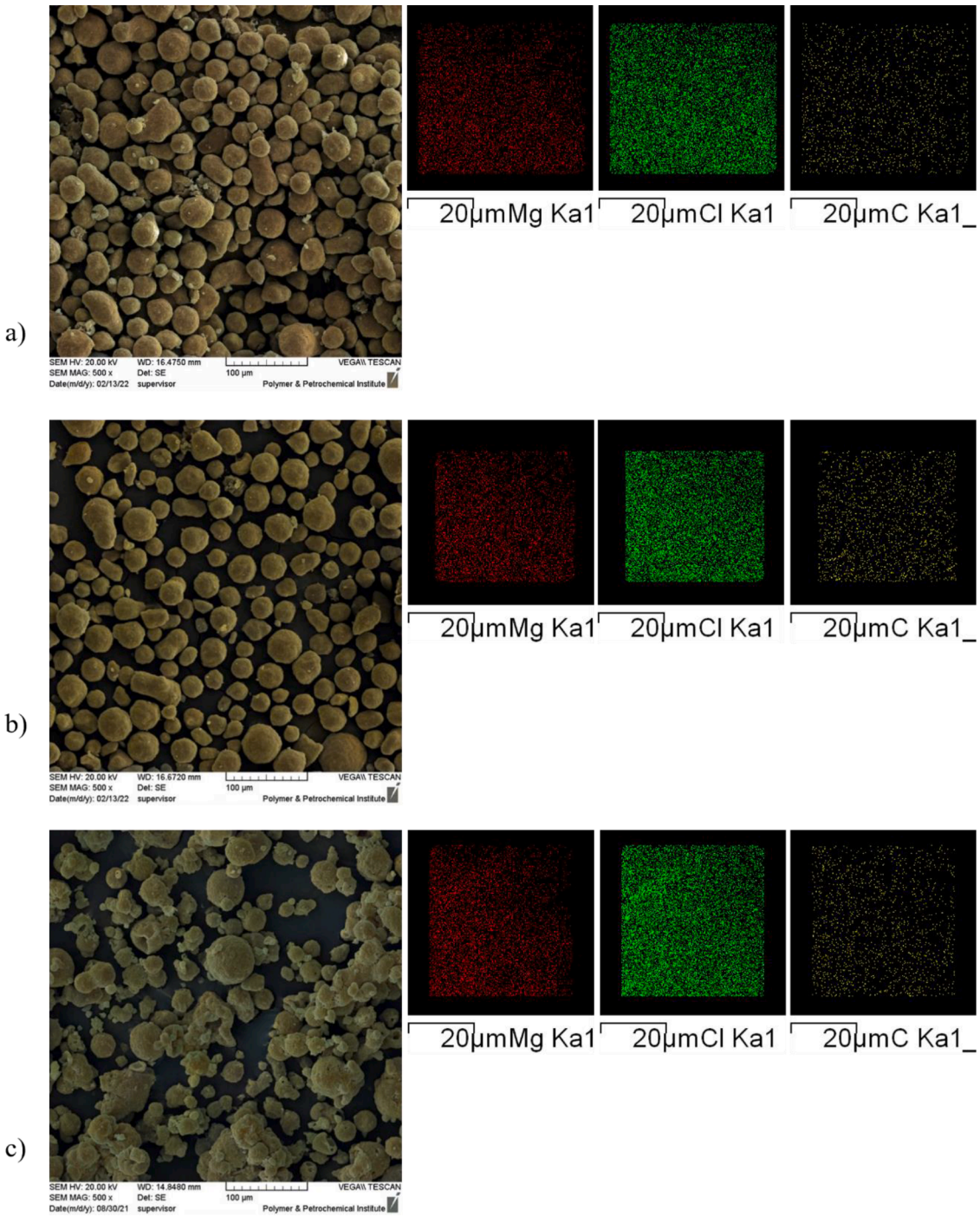

Fig. 3. SEM images and EDX mapping of the adducts (a) Add-22, (b) Add-33 and (c) Add-61.

activated magnesium chloride particles contain $MgCl_2$-monolayers piled irregularly, with exposure of nearly (110) and (104) surfaces [24, 25].

According to the literature, at ambient conditions (pressure and temperature), magnesium chloride exits in the following two crystalline polymorphs: α- and β forms, the first form being the most common form and consisting in $CdCl_2$-type crystals with fcc unit, while β-$MgCl_2$ crystallizes in the CdI_2-type crystals with hcp crystalline unit. In fact, both crystalline forms can be detected in the neat $MgCl_2$. At high pressures and temperatures [73], as well as during $MgCl_2$ modification by Lewis bases and ball milling, the polymorphic concentration ratio can be easily changed. Via the so called processes, the thickening and thinning of the lateral cuts in the crystallites are detected. Despite some previous reports on the broadening of XRD patterns by $MgCl_2$ activation and dealcoholation [11,74] no broadening is observed in XRD spectra of studied adducts here, similar to the findings of some other researchers [75,76]. Another important issue, needing special care, concerns the hygroscopic nature of $MgCl_2$.EtOH adducts. In fact, up to 6 molecules with a Lewis base structure can be bonded to a $MgCl_2$ molecule. It affects not only the morphology and crystalline structure of adduct, but also deteriorates final catalysts performance. According to the Huang et al. [77] appearance of peaks at $2\theta=21$ and 31° can be correlated to the $MgCl_2.H_2O$ structure. The peak at $2\theta=31^\circ$ coincides with the characteristic peak of the (012) lateral plane in $MgCl_2$ structure and cannot

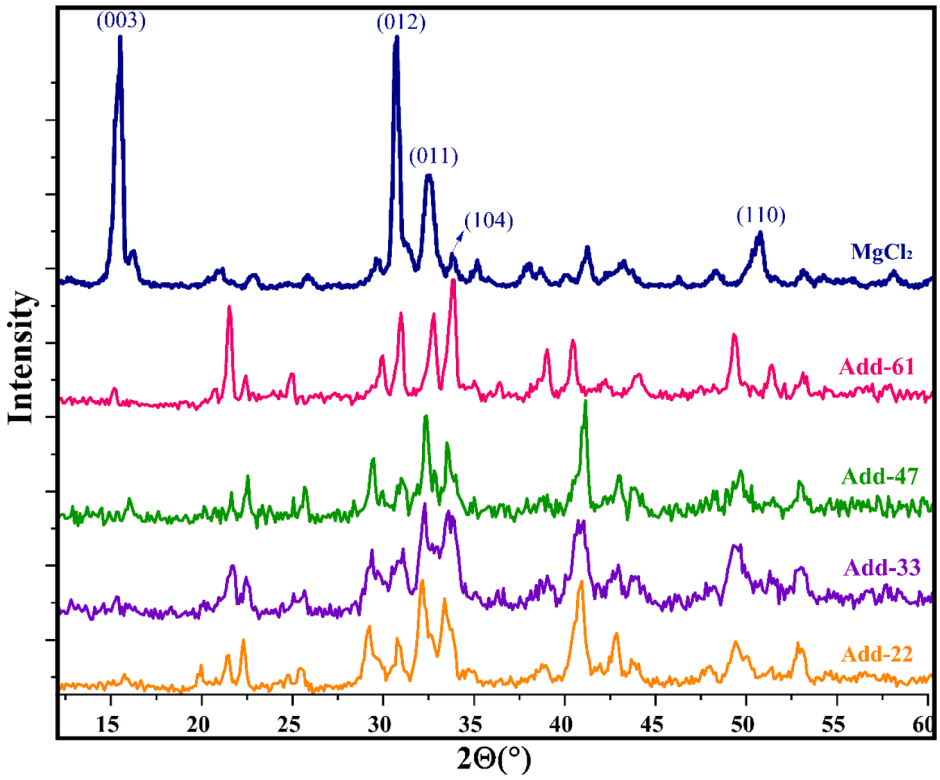

Fig. 4. XRD patterns of the studied adducts and pristine $MgCl_2$.

Table 2
Structural features of the studied adducts and primary $MgCl_2$ obtained from XRD patterns.

Sample label	Parameters	2θ (°) and correlated plane type 16 (003)	31 (012)	32 (011)	34 (104)	50 (110)	α/β ratio
$MgCl_2$	d-Spacing [A°]	5.7	2.9	2.7	2.6	1.8	0.34
	FWHM [°]	0.26	0.24	0.32	0.31	0.41	
	Crystallite size [A°]	308	343	259	268	214	
	Int.%	4340	4331	1959	669	1033	
Add-22	d-Spacing [A°]	5.6	2.9	2.7	2.6	1.8	0.86
	FWHM [°]	0.39	0.82	0.79	0.78	1.25	
	Crystallite size [A°]	206	100	105	106	70	
	Int.%	82	178	334	287	168	
Add-33	d-Spacing [A°]	5.8	2.8	2.7	2.6	1.8	0.94
	FWHM [°]	0.38	0.80	0.53	0.67	0.92	
	Crystallite size [A°]	211	103	156	124	95	
	Int.%	83	180	276	260	185	
Add-47	d-Spacin [A°]	5.7	2.8	2.8	2.7	1.8	1.05
	FWHM [°]	0.36	0.35	0.45	0.58	0.86	
	Crystallite size [A°]	219	135	164	172	178	
	Int.%	85	189	294	287	191	
Add-61	d-Spacin [A°]	5.8	2.8	2.7	2.6	1.8	1.31
	FWHM [°]	0.35	0.34	0.46	0.45	0.41	
	Crystallite size [A°]	229	244	180	183	213	
	Int.%	110	356	361	473	286	

give any hint about the presence of water molecules. On the other hand, the peak at 2θ=21 ° is due to the H_2O, it was not considerable in the XRD spectra of the studied adducts. Therefore, according to the spectra, the water content of the adducts was not considerable. Furthermore, the presence of β- and α-$MgCl_2$ can be rationalized from the peaks at 2θ = 32 and 34° correlated with the hexagonal close packing of the (011) facet in β-$MgCl_2$, and the cubic close packing of (104) facet in α-$MgCl_2$ structure, respectively. The ratio of α to β structures was acquired from the related peaks intensities at 34 and 32° It is clear from Table 2 that α/β ratio enhances from 0.34 in pristine $MgCl_2$ to a value in the range of 0.86–1.31 for various adducts, so that increasing the ethanol content improves the α/β ratio. Additional ethanol appears to provide more structurally deformed $MgCl_2$ structures, however, by thermal treatment; their structure approaches the pristine $MgCl_2$ texture.

The D-spacing, full width at half-maximum (FWHM), crystallite size, and peaks intensity at various 2θ angles of 16, 31, 33, 34 and 50° are gathered in Table 2. Obviously, in the primary $MgCl_2$ the share of the (110) surface is high, which decreases in the adduct samples. Furthermore, the crystallite sizes decrease by ethanol content for all investigated lateral cuts. Moreover, the primary $MgCl_2$ and investigated adducts revealed similar D-spacing in each 2θ angle, while this value varied with the changing 2θ angle.

The disordered extent of the adducts and primary $MgCl_2$ was then evaluated using the Williamson-Hall equation (eq-1) based on the data obtained from XRD analysis.

$$\beta \times \cos(\theta) = C \times \sin(\theta) + \frac{k\lambda}{L} \quad (1)$$

In which, β, λ, k, and L represent the total broadening, the wavelength, a constant (~1), and grain size, respectively. It is worth mentioning this method is a common route to model the broadening [78, 79] of XRD peaks, almost originated from the stacking disorder of the constituent crystals (denoted as C in the formula) and the crystal size. In this method, by plotting β × Cos(θ) versus Sin(θ), C can be obtained from the slope of the fitted line, Table 3. It is clear from the obtained results

Table 3
The Williamson-Hall Equation constants and calculated grain size of the studied adducts.

Sample	Slope	Intercept	Crystallite size (nm)
$MgCl_2$	0.0450	0.0025	72.4
Add-22	0.0074	0.0030	47.6
Add-33	0.0270	0.0033	43.5
Add-47	0.0024	0.0056	32.5
Add-61	0.0022	0.0061	23.8

Table 4
Porosity characteristics of the studied adducts.

Sample label	Total absorbed gas in STP (cm^3/g)	Surface area (m^2/g)	Total pore volume (cm^3/g)	Average pore diameter (nm)	Pore shape
Add-22	3.2	14.1	0.087	24.5	NI[1]
Add-33	2.6	11.4	0.058	20.4	NI[1]
Add-47	1.8	7.9	0.036	18.2	WI[2]
Add-61	1.1	5.0	0.026	16.0	WI[2]

[1] W.I. = Wide Inlet;
[2] N.I. = Narrow Inlet.

that the stacking disorder and crystallite size diminish in adduct samples, compared to neat $MgCl_2$. It is worth mentioning that stacking disorder has direct relationship with particle fragmentation and increases with it.

The porosity of the studied adducts was assessed by N_2 adsorption-desorption measurements method and represented as pore volume, pore diameter, pore shape and total surface area characteristics in Table 4. The pore size distribution of adducts, acquired via BJH curve, revealed an enhancement in pore diameter from 16.0 to 24.5 nm proceeding the thermal dealcolation from Add-61 to Add-22. In deep analyses, only small pores with a diameter ranged from 5 to 25 nm is detected in the related BJH curve, Fig. 5a. On the other hand, in the case of other samples, especially in the most dealcolated one, i.e. Add-22, beside mentioned pores, some larger *meso*-pores with the r_p of 25–40 nm can be clearly observed. These *meso*-pores cause an enhancement in the surface area of the highly dealcolated samples from 5.0 m^2/g in Add-61 to 14.1 m^2/g in Add-22. Using the hysteresis type of BET curves, Fig. 5b, good information about the shape of pores is achieved which is collected in Table 4. In particular, all adducts have a similar amount of hysteresis, but with different pore diameters that reveals a wide inlet type in Add-47 and Add-61, while narrow inlet type in Add-22 and Add-33 samples.

According to the FTIR spectra in Fig. 6, peaks around 3400 cm^{-1} are attributed to O—H stretching, 1408 due to C—C stretching, and 1041 cm^{-1} is correlated to the C—O stretching of ethanol. According to Fig. 6, no considerable variation in the location of the mentioned peaks is detected, which confirms the weak interaction of ethanol as a Lewis acid with $MgCl_2$ support [11]. It is clear that the intensity of peak at 1041 cm^{-1} is lower in the Add-33 sample, when comparing with the other spectra. However, no clear explanation was fount for that. Furthermore, the similar crystalline structure of the studied adducts comprising the same lateral cuts, although with slightly different intensities, imposes the same interaction with ethanol. It confirms the similar FTIR spectra obtained for different adducts with various ethanol extent.

To study the lability of $MgCl_2$ aggregates with ethanol, DFT calculations were run. A systematic study of the interaction of the single $MgCl_2$ unit with a range of 1 to 4 ethanol units, as well as metal clusters of up to 4 $MgCl_2$ units, was carried out. In addition, the calculations were repeated with and without implicit solvent effect, since the real situation is intermediate once the aggregates are used. It is worth mentioning that the structural simplicity from 1 to 4 $MgCl_2$ units leads from a structure with C2v symmetry to one of C2h type, following previous computational studies, where the last $MgCl_2$ unit joins not to form a Mg_4Cl_4 cubic center, but that extending its length, thus repeating 2 units of Mg_4Cl_4 contiguous joined by a square planar Mg_2Cl_2 bridge.

The bond energies in Table 5 allow us to understand that the limit of ethanol molecules is between 3 and 4 units, observing the dichotomy between the optimization results in gas and in solvent. Thus, in solvent 3 units would be the limit, while in gas the monomer of magnesium oxide can reach up to 4 units around it.

Apart from the gain of entropy [80], structurally it is necessary to highlight the fact that with 4 units of ethanol it is only possible the presence of 4 Mg-O bonds only with the $MgCl_2$ monomer, while from the dimer $(MgCl_2)_2$ it is no longer possible, placing one Mg···O interaction to almost 4 Å, but stabilized by 2 of the other ethanol molecules through O···H type H bonds. Therefore, there is a clear trend that magnesium can embrace up to 4 EtOH in the first coordination sphere, however 3 would be the most reliable value.

In addition to the clusters of $MgCl_2$, from one to four units, we proceeded to do the exercise to see how much more unstable it is to arrange the ethanol molecules in a single magnesium center, than not distributing them with the rest of magnesium centers. Thus, for 2 units of magnesium in the gas phase this structure was 11.1 kcal/mol more stable, a value that increases to 9.7 kcal/mol with 4 metal centers. But with this last operation, the multiplier effect of increasing ethanol units is overestimated. In order to avoid this error, if we compare with only 2 units of ethanol, we see that the increase is more modest, of only 1.6 and 1.1 kcal/mol, with 3 or 4 ethanol units, respectively. In addition, knowing that for $(MgCl_2)_4$-$(EtOH)_4$ there is an ethanol ligand not bonded to any magnesium, we wondered if for $(MgCl_2)_3$-$(EtOH)_3$ the same could occur, bearing 2 ethanol ligands on a magnesium center and the third stabilized by strong H-bonds with the two bonded ethanol ligands. Anyway, this species was located 7.4 kcal/mol above in energy. Actually, due to entropy effects [80–82], results with more than 4 ethanol molecules were not included, as they were all found to be higher in energy by at least 6.1 kcal/mol in the best system.

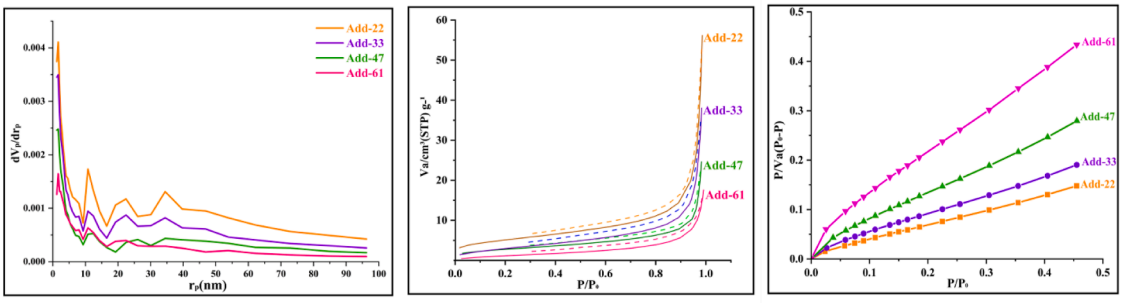

Fig. 5. (a) N_2 adsorption-desorption isotherms plot, (b) BET diagram and (c) BJH curves of the studied adducts.

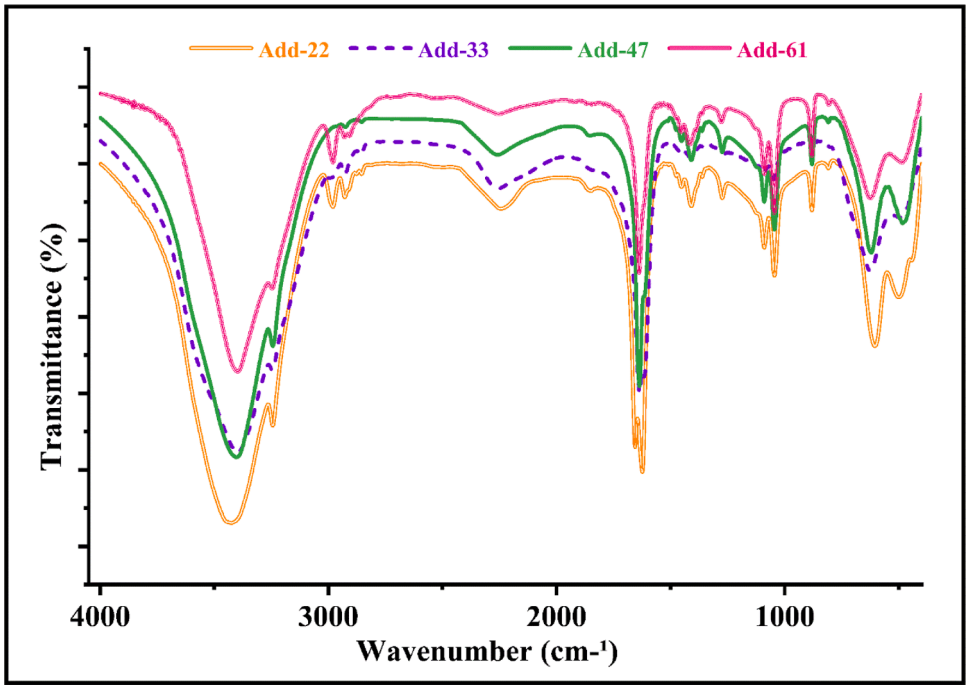

Fig. 6. FTIR spectra of studied adducts containing various amounts of ethanol.

Table 5
Relative Gibbs energies (in kcal/mol) of the $(MgCl_2)_x$ clusters with n EtOH molecules, in gas and in solvent; and Mg-O distances (in Å) in gas.

	ΔG_{gas}	$\Delta G_{solvent}$	d(Mg-O)$_1$	d(Mg-O)$_2$	d(Mg-O)$_3$	d(Mg-O)$_4$
$MgCl_2$	0.0	0.0				
	−19.0	−9.0	2.030			
	−30.4	−15.4	2.062	2.076		
	−34.9	−10.8	2.132	2.126	2.167	
	−43.7	−9.0	2.141	2.111	2.131	2.124
$(MgCl_2)_2$	0.0	0.0				
	−17.6	−9.4	2.031			
	−24.2	−12.7	2.067	2.101		
	−36.3	−16.7	2.132	2.055	2.312	
	−41.2	−15.6	2.082	2.211	2.226	3.712
$(MgCl_2)_3$	0.0	0.0				
	−10.2	−6.1	2.041			
	−28.6	−11.1	2.082	2.062		
	−40.7	−26.5	2.086	2.096	2.129	
	−42.4	−24.3	2.088	2.121	2.083	3.906
$(MgCl_2)_4$	0.0	0.0				
	−19.8	−10.1	2.022			
	−35.9	−18.3	2.045	2.045		
	−40.9	−21.8	2.065	2.063	2.109	
	−45.9	−16.0	2.069	2.024	2.167	3.795

Table 6
Computed IR values (in cm^{-1}) of the $(MgCl_2)_x$ clusters with n EtOH molecules in gas, for the C—O, C—C and O—H moieties.

	n	C-O	C—C	O-H
$MgCl_2$	1	1038.1	1444.3	3771.3
	2	1035.1	1450.1	3742.7
	3	1036.2	1431.9	3729.6
	4	1049.9	1427.9	3666.2
$(MgCl_2)_2$	1	1023.5	1434.3	3790.0
	2	1057.3	1431.3	3654.5
	3	1042.1	1434.3	3701.3
	4	1036.1	1434.4	3589.7
$(MgCl_2)_3$	1	1028.8	1427.8	3757.9
	2	1028.0	1452.1	3764.3
	3	1033.0	1432.9	3754.6
	4	1037.1	1428.3	3616.9
$(MgCl_2)_4$	1	1024.0	1408.3	3762.0
	2	1031.8	1430.5	3773.8
	3	1043.2	1456.2	3432.8
	4	1048.8	1457.6	3464.6

The second and most important computational objective is embodied in the results of Table 6, referring to the IR spectra. The agreement of the results with those arranged in Fig. 7 is such that it was not even necessary to apply the typical correction factor to the computational results. In addition, the structural difference between the optimizations in gas or solvent are minimal (see Table S1), and this is also reflected again in the IR spectra (see Table S2). However, it should be noted that the O—H signal has an error of 5–8% with respect to the experimental values at 3400 cm^{-1}, in line with previous studies. Interestingly, the IR results help corroborate that inserting more ethanol units into the Mg center does not significantly alter the strength of the Mg···O interaction with 1 to 4 units. To give more emphasis to this factor, already structurally verified in Table 5, the results of the MBO (Mayer Bond Order) [83] for the Mg···O interaction reinforce this statement, and thus fixing the role of the ethanol as a Lewis acid [84]. The MBOs of the Mg-O bonds with $MgCl_2$ have values of 0.287 with 1 EtOH; 0.251 and 0.274 with 2 EtOH; 0.248, 0.231 and 0.240 with 3 EtOH; 0.272, 0.268, 0.239 and 0.265 with 4 EtOH; thus, when adding more EtOH molecules there is a slight reduction of the strength with average MBOs of 0.263, 0.240 and 0.261. And with the largest cluster with a non bonded ethanol molecule to any magnesium center, i.e. $(MgCl_2)_4$, there is a remarkable value of 0.157 for the O···H interaction of the non bonded ethanol.

NCI plots developed by Contreras et al. [85,86], and included in Fig. 7 were carried out to reveal that the interaction of $MgCl_2$ derivatives with ethanol is not a simple Mg—O covalent bond [87,88], but also a complex lattice of bonds by hydrogen bonding including a good number of Cl···H interactions. In addition, it is necessary to mention a hydrogen bond of O···H nature of extraordinary strength for $(MgCl_2)_4$-$(EtOH)_4$, with a blue color instead of green [89]. In fact, it is almost assimilable to a bond, and it is also assimilable for the smaller $(MgCl_2)_2$ and $(MgCl_2)_3$ clusters.

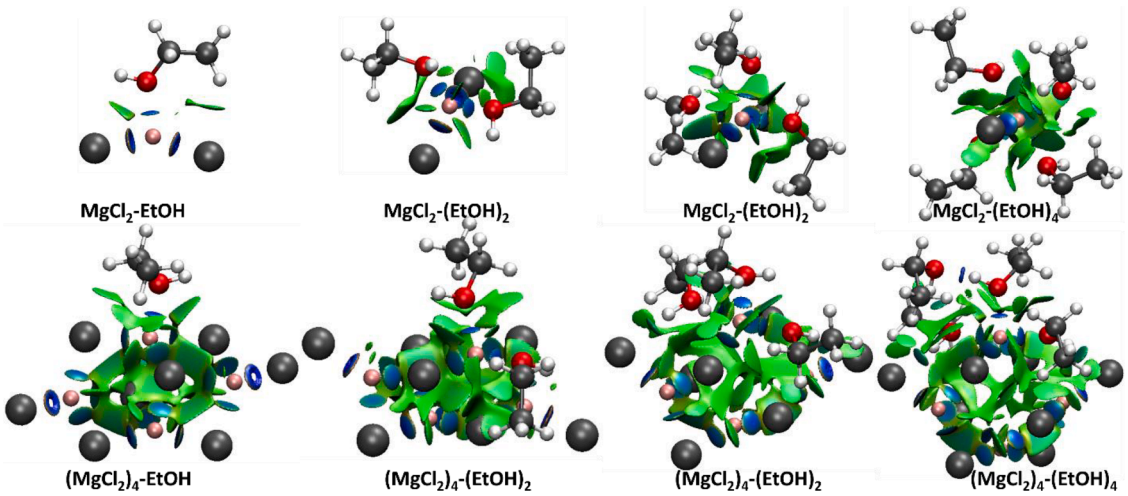

Fig. 7. NCI plots of the interaction of EtOH molecules on $MgCl_2$ and $(MgCl_2)_4$. The isosurface represents a value of 0.5 with a color scale for the reduced density gradient (blue is attractive while red is repulsive).

4. Conclusions

Microstructure of four different $MgCl_2$·nEtOH adducts with $0.6 \leq n \leq 3.2$, prepared through melt quenching method, were analyzed by different techniques. It is worth mentioning that the knowledge about these adducts is not obvious, for example, regarding the disordered modification or the size of the crystalline domains, but it is a step forward as for the first time this paper provides some of the clues following characterization, after the seminal works that tried in the past in the same line [35,44,52–57,71,74,76]. The adducts with $n = 1.8$ and 3.2 revealed multiple EtOH desorption pathway in TGA analysis, revealing both the loosely and semi-tightly bonding of ethanol molecules into the $MgCl_2$ surface. Despite different types of EtOH bindings, studied adducts demonstrated similar FTIR spectra, arisen from not-strong interactions between precursors. In the XRD patterns, although the adducts exhibited similar lateral cuts, however, the ratio of α/β phases of $MgCl_2$ changed by altering EtOH content. Besides, the variation of pore amount and shape by alcohol content was significant. The overall results confirm the importance of alcohol content on the microstructure of $MgCl_2$·nEtOH adducts which influence final Ziegler-Natta catalysts behavior in terms of comonomer incorporation and polymerization kinetic. This is under consideration in our next research, apart from mechanistic calculations by DFT that here perfectly fit with experiments to unveil the importance of both the $MgCl_2$ and EtOH moieties and their consistent interaction in the $MgCl_2$·nEtOH adducts.

CRediT authorship contribution statement

Reza Bazvand: Investigation, Writing – original draft. **Naeimeh Bahri-Laleh:** Conceptualization, Writing – review & editing. **Hossein Abedini:** Investigation, Writing – review & editing, Supervision. **Mehdi Nekoomanesh:** Conceptualization, Writing – review & editing. **Albert Poater:** Investigation, Writing – review & editing, Supervision.

Declaration of Competing Interest

The authors declare that they have no known competing financial interests or personal relationships that could have appeared to influence the work reported in this paper.

Data availability

We have uploaded the Supporting Information file and in addition further information is available upon request, apart from in internal repositories.

Acknowledgments

N.B.-L. is thankful to Iran National Science Foundation for financial support of the work under the grant number of 4006310. A.P. is a Serra Húnter Professor and thanks ICREA Academia 2019, the Ministerio de Ciencia e Innovación for project PID2021–127423NB-I00, and the Generalitat de Catalunya for project 2021SGR623.

Supplementary materials

Supplementary material associated with this article can be found, in the online version, at doi:10.1016/j.molstruc.2023.136098.

References

[1] N. Bahri-Laleh, M. Nekoomanesh-Haghighi, S. Sadjadi, A. Pajouhan, Polyolefin and olefin production in Iran: current and future capacities, Polyolefins J. 3 (2016) 11–22.
[2] D.I.W. Posch, M. Kutz, Polyolefins. Applied Plastics Engineering Handbook, (2nd Edition), William Andrew Publishing, 2017, pp. 27–53.
[3] J. Hernández-Fernández, R. Vivas-Reyes, C.A.T. Toloza, Experimental study of the impact of trace amounts of acetylene and methylacetylene on the synthesis, mechanical and Thermal properties of polypropylene, Int. J. Mol. Sci. 23 (2022) 12148.
[4] P.J. Lutz, F. Peruch, K. Matyjaszewski, M. Möller, 6.14 - Graft copolymers and comb-shaped homopolymers. Polymer Science: A Comprehensive Reference, Elsevier, Amsterdam, 2012, pp. 511–542.
[5] A. Ribas-Massonis, M. Cicujano, J. Duran, E. Besalú, A. Poater, Free-radical photopolymerization for curing products for refinish coatings market, Polymers 14 (2022) 2856 (Basel).
[6] S. Karimi, N. Bahri-Laleh, S. Sadjadi, G. Pareras, M. Nekoomanesh-Haghighi, A. Poater, Pd on nitrogen rich polymer-halloysite nanocomposite as an environmentally benign and sustainable catalyst for hydrogenation of polyalfaolefin based lubricants, J. Ind. Eng. Chem. 97 (2021) 441–451.
[7] M. Stürzel, S. Mihan, R. Mülhaupt, From multisite polymerization catalysis to sustainable materials and all-polyolefin composites, Chem. Rev. 116 (2016) 1398–1433.
[8] Y.V. Kissin, T.E. Nowlin, R.I. Mink, Supported Titanium/Magnesium Ziegler Catalysts for the Production of Polyethylene, in: R. Hoff (Ed.), Handbook of Transition Metal Polymerization Catalysts, 2018.
[9] A. Piovano, E. Groppo, Flexible ligands in heterogeneous catalysts for olefin polymerization: insights from spectroscopy, Coord. Chem. Rev. 451 (2022), 214258.
[10] J.C. Chadwick, F.P.T.J. Van Der Burgt, S. Rastogi, V. Busico, R. Cipullo, G. Talarico, J.J.R. Heere, Influence of Ziegler-Natta catalyst regioselectivity on polypropylene molecular weight distribution and rheological and crystallization behavior, Macromolecules 37 (2004) 9722–9727.
[11] A.; T. Wada, G. Takasao, A. Piovano, M. D'Amore, A. Thakur, P. Chammingkwan, P.C. Bruzzese, M. Terano, B. Civalleri, S. Bordiga, E. Groppo, T Taniike, Revisiting

the identity of δ-$MgCl_2$: part I. structural disorder studied by synchrotron X-ray total scattering, J. Catal. 385 (2020) 76–86.
[12] J.B.P. Soares, T.F.L. McKenna, A conceptual multilevel approach to polyolefin reaction engineering, Can. J. Chem. Eng. 100 (2011) 2432–2474.
[13] M. Shiri, M. Parvazinia, A.A. Yousefi, N. Bahri-Laleh, A. Poater, A novel method for dynamic molecular weight distribution determination in organometallic catalyzed olefin polymerizations, Catalysts 12 (2022) 1130.
[14] F. Farzami, M. Askari, M. Asadi Eraghi, Sensitivity analysis and multi-objective optimization of gas-phase polymerization of propylene using Ziegler-Natta catalysts, Chem. Eng. Res. Des. 184 (2022) 457–472.
[15] C. Chen, Designing catalysts for olefin polymerization and copolymerization: beyond electronic and steric tuning. designing catalysts for olefin polymerization and copolymerization: beyond electronic and steric tuning, Nat. Rev. Chem. 2 (2018) 6–14.
[16] P. Corradini, G. Guerra, L. Cavallo, Do new century catalysts unravel the mechanism of stereocontrol of old Ziegler−Natta catalysts? Acc. Chem. Res. 37 (2004) 231–241.
[17] A. Piovano, T. Wada, A. Amodio, G. Takasao, T. Ikeda, D. Zhu, M. Terano, P. Chammingkwan, E. Groppo, T. Taniike, Formation of highly active Ziegler–Natta catalysts clarified by a multifaceted characterization approach, ACS Catal. 11 (2021) 13782–13796.
[18] I. Kuryndin, S. Kostromin, R. Mamalimov, A. Chervov, A. Grebennikov, S. Bronnikov, Organic solvents effect on the physical and mechanical properties of polyethylene, Polyolefins J. 9 (2022) 25–31.
[19] M.S. Abbas-Abadi, R. Rashedi, A. Sepahi, L. Heydari, A. Farhadi, M. Biglarkhani, The effect of different process parameters on the $TiCl_4$/internal donor/$MgCl_2$/$AlEt_3$ catalytic system using external donor and cyclohexylchloride, Iran. Polym. J. 29 (2020) 659–667.
[20] M. Boero, M. Parrinello, H. Weiss, S. Hüffer, A first principles exploration of a variety of active surfaces and catalytic sites in Ziegler−Natta heterogeneous catalysis, J. Phys. Chem. A 105 (2001) 5096–5105.
[21] M. Humbert, S. Norsic, J. Raynaud, V. Monteil, Activity enhancement of $MgCl_2$-supported Ziegler-Natta catalysts by lewis-acid pre-treatment for ethylene polymerization, Chin. J. Polym. Sci. 37 (2019) 1031–1038.
[22] P. Li, S. Tu, T. Xu, Z. Fu, Z. Fan, The influence of combined external donor and combined cocatalyst on propylene polymerization with a $MgCl_2$-supported Ziegler–Natta catalyst in the presence of hydrogen, J. Appl. Polym. Sci. 132 (2015) 41689.
[23] T. Funako, P. Chammingkwan, T. Taniike, M. Terano, Alternation of pore architecture of Ziegler–Natta catalysts through modification of magnesium ethoxide, Macromol. React. Eng. 9 (2015) 325–332.
[24] M.B. Harney, R.J. Keaton, J.C. Fettinger, L.R. Sita, Living Ziegler-Natta polymerization by early transition metals: synthesis and evaluation of cationic zirconium alkyl complexes bearing β-hydrogens as models for propagating centers, J. Am. Chem. Soc. 128 (2006) 3420–3432.
[25] E. Fazekas, P.A. Lowy, M. Abdul Rahman, A. Lykkeberg, Y. Zhou, R. Chambenahalli, J.A. Garden, Main group metal polymerisation catalysts, Chem. Soc. Rev. 51 (2022) 8793–8814.
[26] S. Escayola, A. Brotons-Rufes, N. Bahri-Laleh, F. Ragone, L. Cavallo, M. Solà, A. Poater, Fluxional bis(phenoxy-imine) Zr and Ti catalysts for polymerization, Theor. Chem. Acc. 140 (2021) 49.
[27] N. Ferrentino, F. Franco, F. Grisi, S. Pragliola, M. Mazzeo, C. Costabile, Ring opening polymerization of lactide promoted by zinc and magnesium complexes with a N-heterocyclic carbene-phenoxy-imine hybrid non-innocent ligand, Mol. Catal. 533 (2022), 112799.
[28] A. Hanifpour, N. Bahri-Laleh, M. Nekoomanesh-Haghighi, A. Poater, 1-Decene oligomerization by new complexes bearing diamine-diphenolates ligands: effect of ligand structure, Appl. Organomet. Chem. 35 (2021) e6227.
[29] A. Hanifpour, N. Bahri-Laleh, M. Nekoomanesh-Haghighi, A. Poater, Coordinative chain transfer polymerization of 1-decene in the presence of a ti-based diamine bis (phenolate) catalyst: a green approach to produce low viscosity PAOs, Green Chem. 22 (2020) 4617–4626.
[30] M. Mehdizadeh, S. Sadjadi, A. Poater, A. Mansouri, N. Bahri-Laleh, Molecular modelling aided catalyst design for PAO oils hydrofinishing, J. Mol. Liq. 352 (2022), 118675.
[31] M. Tabrizi, S. Sadjadi, G. Pareras, M. Nekoomanesh-Haghighi, N. Bahri-Laleh, A. Poater, Efficient hydro-finishing of polyalfaolefin based lubricants under mild reaction condition using Pd on ligands decorated halloysite, J. Colloid Interface Sci. 581 (2021) 939–953.
[32] A. Piovano, M. Signorile, L. Braglia, P. Torelli, A. Martini, T. Wada, G. Takasao, T. Taniike, E. Groppo, Electronic properties of Ti sites in Ziegler–Natta catalysts, ACS Catal. 11 (2021) 9949–9961.
[33] M. Han, Y. Zhao, S. Luo, X. Fan, A. He, Diffusion controlled stereoregular polymerization in granule reactors-reaction kinetic of Pr/Bt sequence polymerization with $TiCl_4$/$MgCl_2$ Ziegler-Natta catalyst, Mol. Catal. 537 (2023), 112938.
[34] T. Charoenpanich, S. Anantawaraskul, J.B.P. Soares, P. Wongmahasirikun, S. Shiohara, Modeling propylene polymerization in a two-reactor system: model development and parameter estimation, Macromol. React. Eng. 16 (2022), 2200027.
[35] I.W. Bassi, F. Polato, M. Calcaterra, J.C.J. Bart, A new layer structure of $MgCl_2$ with hexagonal close packing of the chlorine atoms, Z. Kristallog. Cryst. Mater. 159 (1982) 297–302.
[36] M.N.S. Rad, Highly efficient transition metal-free coupling of acid chlorides with terminal alkynes in [bmim]Br: a rapid route to access ynones using $MgCl_2$, J. Saudi Chem. Soc. 22 (2018) 329–336.
[37] A. Yakimov, J. Xu, K. Searles, W.C. Liao, G. Antinucci, N. Friederichs, V. Busico, C. Copéret, DNP-SENS formulation protocols to study surface sites in Ziegler–Natta catalyst $MgCl_2$ supports modified with internal donors, J. Phys. Chem. C 125 (2021) 15994–16003.
[38] N. Bahri-Laleh, A. Hanifpour, S.A. Mirmohammadi, A. Poater, M. Nekoomanesh-Haghighi, G. Talarico, L. Cavallo, Computational modeling of heterogeneous Ziegler-Natta catalysts for olefins polymerization, Prog. Polym. Sci. 84 (2018) 89–114.
[39] T. Pongchan, P. Praserthdam, B. Jongsomjit, Facile investigation of Ti^{3+} state in Ti-based Ziegler-Natta catalyst with a combination of cocatalysts using electron spin resonance (ESR), Bull. Chem. React. Eng. Catal. 15 (2020) 55–65.
[40] R. Credendino, Y. Minenkov, D. Liguori, F. Piemontesi, A. Melchior, G. Morini, M. Tolazzi, L. Cavallo, Accurate experimental and theoretical enthalpies of association of $TiCl_4$ with typical Lewis bases used in heterogeneous Ziegler–Natta catalysis, Phys. Chem. Chem. Phys. 19 (2017) 26996–27006.
[41] A. Ashuiev, M. Humbert, S. Norsic, J. Blahut, D. Gajan, K. Searles, D. Klose, A. Lesage, G. Pintacuda, J. Raynaud, V. Monteil, C. Copéret, G. Jeschke, Spectroscopic signature and structure of the active sites in Ziegler-Natta polymerization catalysts revealed by electron paramagnetic resonance, J. Am. Chem. Soc. 143 (2021) 9791–9797.
[42] J. Xie, X. Tan, W. Peng, X. Yang, A. He, Effect of $AlEt_2Cl$ on the polymerization of isoprene using $TiCl_4$/$MgCl_2$ type Ziegler-Natta catalyst: a DFT study, Mol. Catal. 502 (2021), 111399.
[43] H. Mori, M. Sawada, T. Higuchi, K. Hasebe, N. Otsuka, M. Terano, Direct observation of $MgCl_2$-supported Ziegler catalysts by high resolution transmission electron microscopy, Macromol. Rapid Commun. 20 (1999) 245–250.
[44] M. D'Amore, K.S. Thushara, A. Piovano, M. Causà, S. Bordiga, E. Groppo, Surface investigation and morphological analysis of structurally disordered $MgCl_2$ and $MgCl_2$/$TiCl_4$ Ziegler–Natta catalysts, ACS Catal. 6 (2016) 5786–5796.
[45] T.B. Mikenas, V.A. Zakharov, M.A. Matsko, Kinetic features of ethylene polymerization over titanium–magnesium catalysts with different structures and morphology, Iran. Polym. J. 31 (2022) 471–484.
[46] Y. Yu, T.F. McKenna, C. Boisson, M.S. Lacerda Miranda, O. Martins Jr, Engineering poly (ethylene-co-1-butene) through modulating the active species by alkylaluminum, ACS Catal. 10 (2020) 7216–7229.
[47] A. Rahbar, M. Nekoomanesh-Haghighi, N. Bahri-Laleh, H. Abedini, Effect of water on the supported Ziegler–Natta catalysts: optimization of the operating conditions by response surface methodology, Catal. Lett. 145 (2015) 1186–1195.
[48] N. Hadian, S. Hakim, M. Nekoomanesh-Haghighi, N. Bahri-Laleh, Storage time effect on dynamic structure of $MgCl_2$.nEtOH adducts in heterogeneous Ziegler-Natta catalysts, Polyolefins J. 1 (2014) 33–41.
[49] N. Bahri-Laleh, A. Correa, S. Mehdipour-Ataei, H. Arabi, M. Nekoomanesh Haghighi, G. Zohuri, L. Cavallo, Moving up and down the titanium oxidation state in Ziegler−Natta catalysis, Macromolecules 44 (2011) 778–783.
[50] A. Shams, M. Mehdizadeh, H. Teimoury, M. Emami, S.A. Mirmohammadi, S. Sadjadi, E. Bardají, A. Poater, N. Bahri-Laleh, Effect of the pore architecture of Ziegler-Natta catalyst on its behavior in propylene/1-hexene copolymerization, J. Ind. Eng. Chem. 116 (2022) 359–370.
[51] M. Masoori, M. Nekoomanesh, S. Posada-Pérez, R. Rashedi, N. Bahri-Laleh, A systematic study on the effect of co-catalysts composition on the performance of Ziegler-Natta catalyst in ethylene/1-butene co-polymerizations, Polymer 261 (2022), 125423 (Guildf).
[52] J.C.J. Bart, W. Roovers, Magnesium chloride—ethanol adducts, J. Mater. Sci. 30 (1995) 2809–2820.
[53] H.S. Cho, W.Y. Lee, Preparation of inorganic $MgCl_2$-alcohol adduct and its application in organometallic HYBRID catalysts for ethylene polymerization, Korean J. Chem. Eng. 19 (2002) 557–563.
[54] H.S. Cho, W.Y. Lee, Synthesis of inorganic $MgCl_2$–alcohol adduct via recrystallization method and its application in supported organometallic catalysts for the polymerization of ethylene with 1-hexene, J. Mol. Catal. A Chem. 191 (2003) 155–165.
[55] R. Jamjah, G.H. Zohuri, J. Vaezi, S. Ahmadjo, M. Nekomanesh, M. Pouryari, Morphological study of spherical $MgCl_2$.nEtOH supported $TiCl_4$ Ziegler-Natta catalyst for polymerization of ethylene, J. Appl. Polym. Sci. 101 (2006) 3829–3834.
[56] X. Jiang, X. Tian, Z. Fan, Crystal structure of ball-milled mixture of sodium chloride and magnesium chloride–ethanol adduct, Mater. Res. Bull. 43 (2008) 343–352.
[57] E. Jalali Dil, S. Pourmahdian, M. Vatankhah, F. Afshar Taromi, Effect of dealcoholation of support in $MgCl_2$-supported Ziegler–Natta catalysts on catalyst activity and polypropylene powder morphology, Polym. Bull. 64 (2010) 445–457.
[58] S. Yousefi, N. Bahri-Laleh, M. Nekoomanesh, M. Emami, S. Sadjadi, S. A. Mirmohammadi, M. Tomasini, E. Bardají, A. Poater, An efficient initiator system containing $AlCl_3$ and supported ionic-liquid for the synthesis of conventional grade polyisobutylene in mild conditions, J. Mol. Liq. 367 (2022), 120381.
[59] V. Busico, R. Cipullo, G. Monaco, G. Talarico, M. Vacatello, J.C. Chadwick, A. Laura Segre, O. Sudmeijer, High-resolution 13C NMR configurational analysis of polypropylene made with $MgCl_2$-supported Ziegler−Natta catalysts. 1. the "Model" system $MgCl_2$/$TiCl_4$−2,6-dimethylpyridine/$Al(C_2H_5)_3$, Macromolecules 32 (1999) 4173–4182.
[60] C. De Rosa, O. Ruiz de Ballesteros, F. Auriemma, G. Talarico, M. Scoti, R. Di Girolamo, A. Malafronte, F. Piemontesi, D. Liguori, I. Camurati, G. Morini, Crystallization behavior of copolymers of isotactic poly(1-butene) with ethylene from Ziegler–Natta catalyst: evidence of the blocky molecular structure, Macromolecules 52 (2019) 9114–9127.

[61] C. De Rosa, O. Ruiz de Ballesteros, R. Di Girolamo, A. Malafronte, F. Auriemma, G. Talarico. M. Scoti, The blocky structure of Ziegler–Natta "random" copolymers: myths and experimental evidence, Polym. Chem. 11 (2020) 34–38.
[62] F. Nouri-Ahangarani, N. Bahri-Laleh, H. Abedini, M. Nekoomanesh, Effect of adduct synthesis parameters on the ethylene polymerization kinetics of Ziegler Natta catalysts, J. Appl. Polym. Sci. (2023) e54053.
[63] M.J. Frisch, G.W. Trucks, H.B. Schlegel, G.E. Scuseria, M.A. Robb, J.R. Cheeseman, G. Scalmani, V. Barone, G.A. Petersson, H. Nakatsuji, X. Li, M. Caricato, A. V. Marenich, J. Bloino, B.G. Janesko, R. Gomperts, B. Mennucci, H.P. Hratchian, J. V. Ortiz, A.F. Izmaylov, J.L. Sonnenberg, D. Williams-Young, F. Ding, F. Lipparini, F. Egidi, J. Goings, B. Peng, A. Petrone, T. Henderson, D. Ranasinghe, V. G. Zakrzewski, J. Gao, N. Rega, G. Zheng, W. Liang, M. Hada, M. Ehara, K. Toyota, R. Fukuda, J. Hasegawa, M. Ishida, T. Nakajima, Y. Honda, O. Kitao, H. Nakai, T. Vreven, K. Throssell, J.A. Montgomery Jr, J.E. Peralta, F. Ogliaro, M.J. Bearpark, J.J. Heyd, E.N. Brothers, K.N. Kudin, V.N. Staroverov, T.A. Keith, R. Kobayashi, J. Normand, K. Raghavachari, A.P. Rendell, J.C. Burant, S.S. Iyengar, J. Tomasi, M. Cossi, J.M. Millam, M. Klene, C. Adamo, R. Cammi, J.W. Ochterski, R.L. Martin, K. Morokuma, O. Farkas, J.B. Foresman, D.J. Fox, Gaussian 16, Revision C.01, Gaussian, Inc., Wallingford CT, 2016.
[64] A.D. Becke, Density-functional thermochemistry. III. the role of exact exchange, J. Chem. Phys. 98 (1993) 5648–5652.
[65] P.J. Stephens, F.J. Devlin, C.F. Chabalowski, M.J. Frisch, Ab initio calculation of vibrational absorption and circular dichroism spectra using density functional force fields, J. Phys. Chem. 98 (1994) 11623–11627.
[66] C.T. Lee, W.T. Yang, R.G. Parr, Development of the Colle–Salvetti correlation-energy formula into a functional of the electron density, Phys. Rev. B 37 (1988) 785–789.
[67] S. Grimme, J. Antony, S. Ehrlich, H. Krieg, A consistent and accurate ab initio parametrization of density functional dispersion correction (DFT-D) for the 94 elements H-Pu, J. Chem. Phys. 132 (2010), 154104.
[68] F. Weigend, R. Ahlrichs, Balanced basis sets of split valence, triple zeta valence and quadruple zeta valence quality for H to Rn: design and assessment of accuracy, Phys. Chem. Chem. Phys. 7 (2005) 3297–3305.
[69] F. Weigend, Accurate Coulomb-fitting basis sets for H to Rn, Phys. Chem. Chem. Phys. 8 (2006) 1057–1065.
[70] A.V. Marenich, C.J. Cramer, D.G. Truhlar, Universal solvation model based on solute electron density and on a continuum model of the solvent defined by the bulk dielectric constant and atomic surface tensions, J. Phys. Chem. B 113 (2009) 6378–6396.
[71] P. Sozzani, S. Bracco, A. Comotti, R. Simonutti, I. Camurati, Stoichiometric compounds of magnesium dichloride with ethanol for the supported Ziegler−Natta catalysis: first recognition and multidimensional MAS NMR study, J. Am. Chem. Soc. 125 (2003) 12881–12893.
[72] M. Fallah, N. Bahri-Laleh, K. Didehban, A. Poater, Interaction of common cocatalysts in Ziegler–Natta-catalyzed olefin polymerization, Appl. Organomet. Chem. 34 (2020) e5333.
[73] E. Stavrou, Y. Yao, J.M. Zaug, S. Bastea, B. Kalkan, Z. Konôpkov, M. Kunz, High-pressure X-ray diffraction, Raman and computational studies of $MgCl_2$ up to 1 Mbar: extensive pressure stability of the β-$MgCl_2$ layered structure, Sci. Rep. 6 (2016) 30631.
[74] A. Piovano, P. Pletcher, M.E.Z. Velthoen, S. Zanoni, S.H. Chung, K. Bossers, M. K. Jongkind, G. Fiore, E. Groppo, B.M. Weckhuysen, Genesis of $MgCl_2$-based Ziegler-Natta catalysts as probed with operando spectroscopy, ChemPhysChem 19 (2018) 2662–2671.
[75] K. Seenivasan, A. Sommazzi, F. Bonino, S. Bordiga, E. Groppo, Spectroscopic investigation of heterogeneous Ziegler–Natta catalysts: tiand Mg chloride tetrahydrofuranates, their interaction compound, and the role of the activator, Chem. Eur. J. 17 (2011) 8648–8656.
[76] V. Di Noto, R. Zannetti, M. Vivani, C. Marega, A. Marigo, S. Bresadola, $MgCl_2$-supported Ziegler-Natta catalysts: a structural investigation by X-ray diffraction and Fourier-transform IR spectroscopy on the chemical activation process through $MgCl_2$-ethanol adducts, Makromol. Chem. 193 (1992) 1653–1663.
[77] Q. Huang, G. Lu, J. Wang, J. Yu, Thermal decomposition mechanisms of $MgCl_2{\cdot}_6H_2O$ and $MgCl_2{\cdot}H_2O$, J. Anal. Appl. Pyrolysis 91 (2011) 159–164.
[78] M.H. Jandaghian, Y. Maddah, A. Sepahi, R. Rashedi, E. Nikzinat, M. Masoori, Probing into effects of support pre-treatment on the polymerization behavior and morphology development of $Mg(OEt)_2$-based Ziegler–Natta catalysts, Catal. Lett. 152 (2022) 1194–1204.
[79] V.D. Mote, Y. Purushotham, B.N. Dole, Williamson-Hall analysis in estimation of lattice strain in nanometer-sized ZnO particles, J. Theor. Appl. Phys. 6 (2012) 1–8.
[80] L. Falivene, V. Barone, G. Talarico, Unraveling the role of entropy in tuning unimolecular vs. bimolecular reaction rates: the case of olefin polymerization catalyzed by transition metals, Mol. Catal. 452 (2018) 138–144.
[81] C.J. Richmond, S. Escayola, A. Poater, Axial ligand effects of Ru-BDA complexes in the O-O bond formation via the I2M bimolecular mechanism in water oxidation catalysis, Eur. J. Inorg. Chem. (2019) 2101–2108.
[82] M. Ahmadi, F. Panahi, N. Bahri-Laleh, M. Sabzi, G. Pareras, B.N. Falcone, A. Poater, pH-Responsive gelation in metallo-supramolecular polymers based on the protic pyridinedicarboxamide ligand, Chem. Mater. 13 (2022) 6155–6169.
[83] I. Mayer, Charge, bond order and valence in the AB initio SCF theory, Chem. Phys. Lett. 97 (1983) 270–274.
[84] A. Hanifpour, N. Bahri-Laleh, M. Nekoomanesh-Haghighi, A. Poater, Group IV diamine bis(phenolate) catalysts for 1-decene oligomerization, Mol. Catal. 493 (2020), 111047.
[85] E.R. Johnson, S. Keinan, P. Mori-Sanchez, J. Contreras-Garcia, A.J. Cohen, W. T. Yang, Revealing noncovalent interactions, J. Am. Chem. Soc. 132 (2010) 6498–6506.
[86] J. Contreras-Garcia, E.R. Johnson, S. Keinan, R. Chaudret, J.P. Piquemal, D. N. Beratan, W.T. Yang, NCIPLOT: a program for plotting noncovalent interaction regions, J. Chem. Theory Comput. 7 (2011) 625–632.
[87] J. Poater, M. Gimferrer, A. Poater, Covalent and ionic capacity of MOFs to Sorb small gas molecules, Inorg. Chem. 57 (2018) 6981–6990.
[88] S. Gharajedaghi, Z. Mohamadnia, E. Ahmadi, M. Marefat, G. Pareras, S. Simon, A. Poater, N. Bahri-Laleh, Experimental and DFT study on titanium-based half-sandwich metallocene catalysts and their application for production of 1-hexene from ethylene, Mol. Catal. 509 (2021), 111636.
[89] L. Mweene, G.P. Khanal, J. Kawala, S. Subramanian, Investigations into the flotation of molybdenite in the presence of chalcopyrite using (3S,4S,5S,6R)-3,4,5,6-tetrahydroxyoxane-2-carboxylate acid as a novel selective depressant: an experimental and theoretical perspective, J. Mol. Liq. 368 (2022), 120661.